Received January 1996
Accepted April 1996

Asymptotic and numerical analysis of vertical, planar liquid sheets subject to London-van der Waals forces

J.I. Ramos
Departamento de Lenguajes y Ciencias de la Computación, Universidad de Málaga, Málaga, Spain

Introduction

Coating flows are useful for covering a large surface area with one or more thin, uniform liquid layers. The liquid film is subsequently dried or cured and, often, serves to protect or decorate the substrate[1]. Planar liquid sheets falling vertically under gravity and guided by two vertical wires have been proposed to coat a horizontally moving substrate[2], and are of importance in film casting processes. The fluid dynamics of these sheets is amenable to long-wave asymptotic analysis if the fluid is incompressible (constant density) and isothermal, and if the Reynolds number is small[3].

For sufficiently thin planar liquid sheets, long-range London-van der Waals attractions[4, 5] may be important and may cause the rupture of these sheets. In this paper, the effects of only London-van der Waals body forces on the fluid dynamics of thin, vertical, planar liquid sheets at low Reynolds numbers are considered, while electrostatic and double-layer forces are disregarded. The sheets are assumed to be thin enough for the London-van der Waals forces to be operative, and sufficiently thick that a continuum theory of the liquid is applicable.

London-van der Waals forces have been the subject of extensive research in recent years because of their importance in the rupture of thin films on solid substrates[6], thinning of the dimpled liquid films formed as drops or bubbles approach fluid-fluid interfaces[7], free films, soap films, coalescence of droplets or emulsions, etc. In all these cases, the rupture of the film results from an amplification of spontaneous fluctuations by long range molecular forces due to the London-van der Waals attraction. These forces are always operative in very thin films, i.e., films of thickness ranging from 10nm to 100nm.

The stability of thin, planar liquid sheets is characterized by two instability modes: the axisymmetric, varicose, peristaltic or squeezing mode, and the antisymmetric, undulation or bending mode. The important mode for the rupture of the film is the varicose one. The film rupture, however, may not be analysed accurately by means of linear stability analysis since its validity requires that the film perturbations be small.

International Journal of Numerical Methods for Heat & Fluid Flow
Vol. 7 No. 1, 1997, pp. 42-62.

In this paper, an asymptotic, long-wave analysis of thin, planar liquid sheets subjected to London-van der Waals body forces is presented. This analysis shows that, in contrast to thin films on solid substrates[6], the leading order flow is governed by two partial differential equations for the leading order film thickness and axial velocity. Since the flow is characterized by the Reynolds, Froude and capillary numbers and the Hamaker constant, a, detailed asymptotic analysis is presented for small Reynolds and capillary numbers, small Hamaker's constants, and large Froude numbers in order that the effects of gravity, London-van der Waals forces, surface tension and viscosity appear at the same order in the perturbation parameter. Analytical solutions of the leading order equations are obtained for very large capillary numbers, i.e. small surface tension. A linear, temporal stability analysis is also performed in order to determine the effects of surface tension, viscosity and London-van der Waals forces on the stability of thin, vertical, planar liquid sheets. Finally, numerical methods are employed to solve the non-linear equations corresponding to steady, vertical, planar liquid sheets, in order to determine the effects of the Froude and Reynolds numbers, and Hamaker's constant on plane stagnation flows and film casting processes. Comparisons between the results presented in this paper and those of reference[3], where planar liquid sheets at low Reynolds numbers were studied in the absence of London-van der Waals forces, illustrate the effects of the Hamaker constant on the fluid dynamics of these sheets.

Formulation

Consider a planar liquid sheet infinite in the z direction so that its motion may be considered to be two-dimensional in the (x, y) plane, and assume that the fluid is incompressible (constant density), isothermal and Newtonian so that the conservation equations of mass and linear momentum can be written as

$$\frac{\partial u^*}{\partial x^*} + \frac{\partial v^*}{\partial y^*} = 0, \tag{1}$$

$$\rho^* \left(\frac{\partial u^*}{\partial t^*} + u^* \frac{\partial u^*}{\partial x^*} + v^* \frac{\partial u^*}{\partial y^*} \right) = -\frac{\partial p^*}{\partial x^*} + \mu^* \left(\frac{\partial^2 u^*}{\partial x^{*2}} + \frac{\partial^2 u^*}{\partial y^{*2}} \right) + \rho^* g^* - \frac{\partial W^*}{\partial x^*}, \tag{2}$$

$$\rho^* \left(\frac{\partial v^*}{\partial t^*} + u^* \frac{\partial v^*}{\partial x^*} + v^* \frac{\partial v^*}{\partial y^*} \right) = -\frac{\partial p^*}{\partial y^*} + \mu^* \left(\frac{\partial^2 v^*}{\partial x^{*2}} + \frac{\partial^2 v^*}{\partial y^{*2}} \right) - \frac{\partial W^*}{\partial y^*}; \tag{3}$$

where t is time; u, and v are the axial and transverse velocity components of the liquid, respectively; x and y are the axial and transverse co-ordinates, respectively; ρ and μ, are the fluid's density and dynamic viscosity, respectively; p is the pressure; g is the gravitational acceleration; W is the potential of the body forces; and the asterisk denotes dimensional variables.

Equations (1)-(3) are subjected to symmetry conditions at the planar sheet's axis, i.e.

$$\frac{\partial u^*}{\partial y^*}(x^*, 0, t^*) = \frac{\partial p^*}{\partial y^*}(x^*, 0, t^*) = v^*(x^*, 0, t^*) = 0, \tag{4}$$

and kinematic and dynamic boundary conditions at the sheet's interface $y^* = h^*(x^*, t^*)$ where h^* denotes the local half-width of the planar liquid sheet. The kinematic condition establishes that the liquid-surroundings interface is a material surface where the shear stress is continuous, and the jump in normal stresses across the interface must be balanced by surface tension. The kinematic and dynamic boundary conditions at the planar liquid sheet's interface, i.e. at $y^* = h^*(x^*, t^*)$, are

$$v^* = \frac{\partial h^*}{\partial t^*} + u^* \frac{\partial h^*}{\partial x^*}, \tag{5}$$

$$2\mu^* \left(\frac{\partial v^*}{\partial y^*} - \frac{\partial u^*}{\partial x^*} \right) \frac{\partial h^*}{\partial x^*} + \mu^* \left(\frac{\partial u^*}{\partial y^*} + \frac{\partial v^*}{\partial x^*} \right) \left(1 - \left(\frac{\partial h^*}{\partial x^*} \right)^2 \right) = 0, \tag{6}$$

$$2\mu^* \frac{\partial u^*}{\partial x^*} \left(\frac{\partial h^*}{\partial x^*} \right)^2 - p^* \left(1 + \left(\frac{\partial h^*}{\partial x^*} \right)^2 \right) + 2\mu^* \frac{\partial v^*}{\partial y^*} - 2\mu^* \left(\frac{\partial u^*}{\partial y^*} + \frac{\partial v^*}{\partial x^*} \right) \frac{\partial h^*}{\partial x^*} = -p_e^* \left(1 + \left(\frac{\partial h^*}{\partial x^*} \right)^2 \right) + \sigma^* \frac{\frac{\partial^2 h^*}{\partial x^{*2}}}{(1 + (\frac{\partial h^*}{\partial x^*})^2)^{\frac{1}{2}}}, \tag{7}$$

where σ^* denotes the liquid's surface tension and p_e^* is the pressure of the surroundings which have been assumed to be dynamically passive. This assumption is justified since, if the surroundings are gases, they have, in general, smaller density and dynamic viscosity than those of liquids. This implies that the surrounding gases may not introduce strong velocity variations on each cross-section of the liquid sheet although they may affect its dynamics.

In addition to the above symmetry, kinematic and dynamic boundary conditions, upstream and downstream boundary conditions are required to fully specify and determine the dynamics of the planar liquid sheet. For planar sheets emerging from a nozzle, the upstream boundary conditions i.e., the boundary conditions at the nozzle exit, are rather complex since the flow relaxes from channel, i.e. no-slip conditions, to the kinematic and dynamic boundary conditions given by equations (5)-(7). Moreover, the body forces may be different for the flow within the nozzle than for the free falling sheet on account of the solid walls of the nozzle and the free surfaces.

In this paper, the equations governing the fluid dynamics of thin, planar liquid sheets are derived without accounting for the upstream and downstream boundary conditions, and by assuming that the body forces are those of London-van der Waals, i.e.

$$W^*(\mathbf{r}) = \int w(|\mathbf{r}^* - \mathbf{r}^{*'}|)\rho(\mathbf{r}^{*'})d\mathbf{r}^{*'}, \tag{8}$$

where

$$w(|\mathbf{r}^* - \mathbf{r}^{*'}|) \approx \frac{\Lambda^*}{(|\mathbf{r}^* - \mathbf{r}^{*'}|)^6} \tag{9}$$

and Λ^* is the London-van der Waals constant.

In general, W^* is a function of t^*, x^* and y^*. For thin planar liquid sheets, however, the potential of body forces may be simplified and replaced by the following approximation

$$W \approx \frac{A^*}{6\pi(2h^*)^3} \tag{10}$$

where A^* denotes the Hamaker constant.

For thin, planar liquid sheet, $\epsilon = h_0^*/L^* << 1$ where h_0^* and L^* are the characteristic thickness and axial distance, respectively. The above condition on ϵ also corresponds to a long-wave analysis of the governing equations.

We now introduce the following non-dimensional variables

$$h = h^*/h_0^*, \qquad x = x^*/L^*, \qquad y = y^*/h_0^*,$$

$$u = u^*/u_0^*, \qquad p = p^* L^*/\mu^* u_0^*, \qquad t = t^* u_0^*/L^*, \tag{11}$$

so that the continuity equation may be written as

$$\frac{\partial u}{\partial x} + \frac{\partial v}{\partial y} = 0, \tag{12}$$

where

$$v^* = \epsilon u_0^* v. \tag{13}$$

The non-dimensional linear momentum equations may be written as

$$\epsilon Re\left(\frac{\partial u}{\partial t} + u\frac{\partial u}{\partial x} + v\frac{\partial u}{\partial y}\right) = -\epsilon^2\frac{\partial p}{\partial x} + \epsilon^2\frac{\partial^2 u}{\partial x^2} + \frac{\partial^2 u}{\partial y^2} + \frac{Re}{Fr} + \frac{3\epsilon A_H}{h^4}\frac{\partial h}{\partial x}, \tag{14}$$

$$\epsilon Re\left(\frac{\partial v}{\partial t} + u\frac{\partial v}{\partial x} + v\frac{\partial v}{\partial y}\right) = -\frac{\partial p}{\partial y} + \epsilon^2\frac{\partial^2 v}{\partial x^2} + \frac{\partial^2 v}{\partial y^2}, \tag{15}$$

while the non-dimensional kinematic and boundary conditions read as

$$v(x,h,t) = \frac{\partial h}{\partial t} + u(x,h,t)\frac{\partial h}{\partial x}, \tag{16}$$

$$2\epsilon^2\left(\frac{\partial v}{\partial y} - \frac{\partial u}{\partial x}\right)\frac{\partial h}{\partial x} + \left(\frac{\partial u}{\partial y} + \epsilon^2\frac{\partial v}{\partial x}\right)\left(1 - \epsilon^2\left(\frac{\partial h}{\partial x}\right)^2\right) = 0, \tag{17}$$

$$2\epsilon^2\frac{\partial u}{\partial x}\left(\frac{\partial h}{\partial x}\right)^2+(p_e-p)\left(1+\epsilon^2\left(\frac{\partial h}{\partial x}\right)^2\right)+2\frac{\partial v}{\partial y}$$
$$-2\left(\frac{\partial u}{\partial y}+\epsilon^2\frac{\partial v}{\partial x}\right)\frac{\partial h}{\partial x}=\frac{\epsilon}{Ca}\frac{\frac{\partial^2 h}{\partial x^2}}{(1+\epsilon^2(\frac{\partial h}{\partial x})^2)^{\frac{1}{2}}}, \tag{18}$$

where

$$Fr=\frac{u_0^{*2}}{g^*h_0^*},\qquad Re=\frac{\rho^*u_0^*h_0^*}{\mu^*},\qquad Ca=\frac{\mu^*u_0^*}{\sigma^*},\qquad A_H=\frac{A^*}{48\pi\mu^*u_0^*h_0^{*2}} \tag{19}$$

are the Froude, Reynolds and capillary numbers, respectively, and A_H is the non-dimensional Hamaker constant.

For large Froude and small Reynolds numbers, small London-van der Waals forces, and large surface tension, we assume that

$$Fr=\frac{F}{\epsilon},\ Re=\epsilon R,\ Ca=\epsilon C,\ A_H=\epsilon A, \tag{20}$$

where A, C, F and R are of O(1), so that linear momentum equations, i.e. equations (13) and (14), become

$$\epsilon^2R\left(\frac{\partial u}{\partial t}+u\frac{\partial u}{\partial x}+v\frac{\partial u}{\partial y}\right)=-\epsilon^2\frac{\partial p}{\partial x}+\epsilon^2\frac{\partial^2 u}{\partial x^2}+\frac{\partial^2 u}{\partial y^2}+\epsilon^2\frac{R}{F}+\frac{3\epsilon^2A}{h^4}\frac{\partial h}{\partial x}, \tag{21}$$

$$\epsilon^2R\left(\frac{\partial v}{\partial t}+u\frac{\partial v}{\partial x}+v\frac{\partial v}{\partial y}\right)=-\frac{\partial p}{\partial y}+\epsilon^2\frac{\partial^2 v}{\partial x^2}+\frac{\partial^2 v}{\partial y^2}. \tag{22}$$

whereas the normal stress boundary condition becomes

$$2\epsilon^2\frac{\partial u}{\partial x}\left(\frac{\partial h}{\partial x}\right)^2+(p_e-p)\left(1+\epsilon^2\left(\frac{\partial h}{\partial x}\right)^2\right)+2\frac{\partial v}{\partial y}$$
$$-2\left(\frac{\partial u}{\partial y}+\epsilon^2\frac{\partial v}{\partial x}\right)\frac{\partial h}{\partial x}=\frac{1}{C}\frac{\frac{\partial^2 h}{\partial x^2}}{(1+\epsilon^2(\frac{\partial h}{\partial x})^2)^{\frac{1}{2}}}. \tag{23}$$

The liquid sheet's velocity components, pressure and half-width may be expressed as

$$u=u_0+\epsilon^2u_2+O(\epsilon^4), \tag{24}$$

$$v=v_0+\epsilon^2v_2+O(\epsilon^4), \tag{25}$$

$$p=p_0+\epsilon^2p_2+O(\epsilon^4), \tag{26}$$

$$h=h_0+\epsilon^2h_2+O(\epsilon^4). \tag{27}$$

Substitution of equations (24)-(27) into the continuity (equation (12)) and linear momentum (equations (21) and (22)) equations yields the following sequence of problems.

To O(ϵ^0):

$$\frac{\partial u_0}{\partial x} + \frac{\partial v_0}{\partial y} = 0, \tag{28}$$

$$\frac{\partial^2 u_0}{\partial y^2} = 0, \tag{29}$$

$$-\frac{\partial p_0}{\partial y} + \frac{\partial^2 v_0}{\partial y^2} = 0. \tag{30}$$

To O(ϵ^2):

$$\frac{\partial u_2}{\partial x} + \frac{\partial v_2}{\partial y} = 0, \tag{31}$$

$$R\left(\frac{\partial u_0}{\partial t} + u_0\frac{\partial u_0}{\partial x} + v_0\frac{\partial u_0}{\partial y}\right) = -\frac{\partial p_0}{\partial x} + \frac{\partial^2 u_0}{\partial x^2} + \frac{R}{F} + \frac{\partial^2 u_2}{\partial y^2} + \frac{3A}{h_0^4}\frac{\partial h_0}{\partial x}, \tag{32}$$

$$R\left(\frac{\partial v_0}{\partial t} + u_0\frac{\partial v_0}{\partial x} + v_0\frac{\partial v_0}{\partial y}\right) = -\frac{\partial p_2}{\partial y} + \frac{\partial^2 v_0}{\partial x^2} + \frac{\partial^2 v_2}{\partial y^2}. \tag{33}$$

Substitution of equations (24)-(27) into the kinematic (cf. equation (16)) and dynamic boundary conditions (cf. equation (23)), and expansion of the variables at (x, h, t) in Taylor's series around (x, h_0, t) yield the following sequence problems.

To O(ϵ^0):

$$v_0(x, h_0, t) = \frac{\partial h_0}{\partial t} + u_0(x, h_0, t)\frac{\partial h_0}{\partial x}, \tag{34}$$

$$\frac{\partial u_0(x, h_0, t)}{\partial y} = 0, \tag{35}$$

$$(p_e - p_0) + 2\frac{\partial v_0}{\partial y} - 2\frac{\partial h_0}{\partial x}\frac{\partial u_0}{\partial y} = \frac{1}{C}\frac{\partial^2 h_0}{\partial x^2}, \tag{36}$$

To O(ϵ^0):

$$v_2(x, h_0, t) + h_2\frac{\partial v_0(x, h_0, t)}{\partial y} = \frac{\partial h_2}{\partial t} + \left(u_2(x, h_0, t) + h_2\frac{\partial u_0(x, h_0, t)}{\partial y}\right)\frac{\partial h_0}{\partial x} + u_0(x, h_0, t)\frac{\partial h_2}{\partial x}, \tag{37}$$

$$2\left(\frac{\partial v_0}{\partial y} - \frac{\partial u_0}{\partial y}\right)\frac{\partial h_0}{\partial x} - \frac{\partial u_0}{\partial y}\left(\frac{\partial h_0}{\partial x}\right)^2 + \frac{\partial u_2}{\partial y} + \frac{\partial v_0}{\partial x} + h_2\frac{\partial^2 u_0}{\partial y^2} = 0. \tag{38}$$

The boundary conditions at the symmetry axis can be expressed as (cf. equation (4))

$$v_i = \frac{\partial u_i}{\partial y} = \frac{\partial p_i}{\partial y} = 0, \qquad i = 0, 1, 2, ..., \ at \qquad y = 0. \tag{39}$$

The solution of equation (29) subject to equation (39) is

$$u_0 = B(x, t), \tag{40}$$

i.e. to leading order, the axial velocity component is independent of the transverse co-ordinate.

The solutions of equations (30) and (28) subject to equation (39) are, respectively,

$$p_0 = D(x, t), \qquad v_0 = -B'(x, t)y, \tag{41}$$

where the prime denotes partial differentiation with respect to *x*.

The solution of equations (32) and (33) subject to equation (39) are, respectively,

$$u_2 = \frac{E(x, t)}{2}y^2 + G(x, t), \qquad v_2 = -\frac{E'(x, t)}{6}y^3 - G'(x, t)y, \tag{42}$$

where

$$E = R\left(\frac{\partial B}{\partial t} + B\frac{\partial B}{\partial x}\right) + \frac{\partial D}{\partial x} - \frac{R}{F} - \frac{\partial^2 B}{\partial x^2} - \frac{3A}{h_0^4}\frac{\partial h_0}{\partial x}, \tag{43}$$

and G(x, t) is a function which may be determined at higher order in the asymptotic expansion.

Substitution of equations (40) and (41) into equation (34) yields

$$\frac{\partial h_0}{\partial t} + \frac{\partial (Bh_0)}{\partial x} = 0, \tag{44}$$

while equation (36) results in

$$D = p_e - 2B' - \frac{1}{C}\frac{\partial^2 h_0}{\partial x^2}. \tag{45}$$

Finally equation (38) becomes

$$R\left(\frac{\partial (Bh_0)}{\partial t} + \frac{\partial (B^2 h_0)}{\partial x}\right) = \frac{R}{F}h_0 + 4\frac{\partial}{\partial x}(h_0\frac{\partial B}{\partial x}) + \frac{h_0}{C}\frac{\partial^3 h_0}{\partial x^3} + \frac{3A}{h_0^3}\frac{\partial h_0}{\partial x}. \tag{46}$$

In the absence of attractive London-van der Waals body forces, equation (46) reduces to that of the viscous-gravity-capillary planar liquid sheets derived by Taylor in the appendix to Brown[2,3]. Equation (46) is also valid for horizontal, planar liquid sheets if the first term in its right-hand-side is set to zero. In fact, Erneux and Davis[8] recently derived analogous expressions to equations (44) and (46) using a long-wave theory for horizontal, planar liquid sheets.

Remark. An equation identical to equation (46) may be obtained if only the velocity components and the pressure are expanded as indicated in equations

(24)-(26). If this expansion is used, h_0 in equation (46) must be replaced by h. Note that equations (44) and (46) correspond to long-wave approximations which are not valid near boundaries; however, they will be used in the "Presentation of results" section to determine the fluid dynamics of steady, plane stagnation flows and steady film casting processes, and will be assumed to be valid at both the upstream and downstream boundaries. At these boundaries, the London-van der Waals forces may not obey as a simple expression as equation (10); however, such an expression will be assumed to be valid up to the boundaries.

Viscous-gravity liquid sheets. If there is no surface tension, i.e., $Ca = \infty$, or if surface tension is small, i.e., $Ca = C/\epsilon$ where C = $O(1)$, use of the asymptotic expansions given by equations (24)-(27) yields equation (44) and equation (46) without the third term on the right-hand side of that equation.

Viscous liquid sheets in zero gravity. If there is no surface tension, i.e. $Ca = \infty$, or if surface tension is small, i.e. $Ca = C/\epsilon$ where $C = O(1)$, and $Fr = \infty$, use of the asymptotic expansions given by equations (24)-(27) yields equation (44) and equation (46) without the first term on the right-hand-side of that equation. This result also applies in microgravity environments when $Fr = F/\epsilon^3$ where $F = O(1)$.

Other body forces. As indicated by, for example, Israelachvili[4], Derjaguin *et al.*[5] and Slattery[7], the London-van der Waals body force potential may be expressed as

$$W^* = -\frac{B^*_{LW}}{h^{*n}}, \tag{47}$$

where the values of B^*_{LW} and n depend on the film thickness. For thin films, B^*_{LW} generally decreases whereas n increases as the film thickness is increased. Of course, the effects of the London-van der Waals potential are negligible for thick films.

For the potential given by equation (47), the fourth term in the right-hand side of equation (46) is to be replaced by $\frac{nA}{h_0^n}\frac{\partial h_0}{\partial x}$ where $A = \frac{B^*_{LW}}{\mu^* u_0^* h_0^{n-1}}$.

Steady state solutions

For steady, planar liquid sheets, equations (44) and (46) become

$$Bh_0 = C_1, \qquad RC_1\frac{dB}{dx} = \frac{R}{F}h_0 + 4\frac{d}{dx}(h_0\frac{dB}{dx}) + \frac{h_0}{C}\frac{d^3h_0}{dx^3} + \frac{3A}{h_0^3}\frac{dh_0}{dx}, \tag{48}$$

where C_1 is an integration constant which can be set to one without loss of generality. In general, it is impossible to get the analytical solution to equation (46) except in some particular cases, some of which are analysed in the following paragraphs.

$Ca = \infty$ and $Re = 0$. In this case, equation (48) may be integrated to obtain

$$4B'h_0 - \frac{3A}{2h_0^2} = \alpha, \tag{49}$$

where α is an integration constant. Substitution of $h_0 = 1/B$ into equation (49) and integration of the resulting equation yield

$$\frac{B}{(1+\gamma B^2)^{\frac{1}{2}}} = \frac{\alpha x}{4} + \beta, \tag{50}$$

where β is another integration constant and $\gamma = \frac{3A}{2\alpha}$. Equation (50) is also valid if $Ca = \epsilon^{-1}C$ where $C = O(1)$.

$Ca = \infty$ and $Fr = \infty$. In this case, integration of equation (48) yields

$$RB = 4B'h_0 - \frac{3A}{2h_0^2} + \alpha. \tag{51}$$

Substitution of $h_0 = 1/B$ into equation (51) and integration of the resulting equation yield[9]

$$\frac{3Ax}{8} + \beta = \frac{1}{2c} ln \frac{B^2}{|B^2 + bB + c|} - \frac{b}{c|b^2 - 4c|^{\frac{1}{2}}} H(B; b, c), \tag{52}$$

where

$$H(B; b, c) = \frac{1}{2} ln \frac{2B + b - (b^2 - 4c)^{\frac{1}{2}}}{2B + b + (b^2 - 4c)^{\frac{1}{2}}}, \qquad for \qquad b^2 > 4c, \tag{53}$$

$$H(B; b, c) = arctan \frac{2B + b}{(4c - b^2)^{\frac{1}{2}}}, \qquad for \qquad b^2 < 4c, \tag{54}$$

where

$$b = \frac{2R}{3A}, \qquad c = -\frac{2\alpha}{3A}. \tag{55}$$

If $b^2 = 4c$, the solution of equation (51) may be written as

$$\frac{3Ax}{8} + \beta = \frac{1}{c} \left(ln \frac{B}{|B + \frac{b}{2}|} + \frac{b}{2} \frac{1}{B + \frac{b}{2}} \right). \tag{56}$$

Equations (52) and (56) also hold for $Ca = \epsilon^{-1}C$ and $Fr = \epsilon^{-3}F$ where C and F are $O(1)$.

General case. For arbitrary values of the Froude, Reynolds and capillary numbers and Hamaker's constant, equation (48) may be written as

$$-\frac{R}{h_0^2}\frac{dh_0}{dx} = -4\frac{d}{dx}\left(\frac{1}{h_0}\frac{dh_0}{dx}\right) + \frac{h_0}{C}\frac{d^3h_0}{dx^3} + \frac{3A}{h_0^3}\frac{dh_0}{dx} + \frac{R}{F}h_0, \tag{57}$$

which is a third-order, non-linear, ordinary differential equation. The order of this equation can be reduced by one by means of the transformation $q = \frac{dh_0}{dx}$ which yields

$$-\frac{Rq}{h_0^2} = -4q\frac{d}{dh_0}(\frac{q}{h_0}) + \frac{h_0 q}{C}\frac{d}{dh_0}(h_0\frac{dq}{dh_0}) + \frac{3Aq}{h_0^3} + \frac{R}{F}h_0. \tag{58}$$

Equation (58) is still non-linear and its solution may be obtained numerically. It must be noted that, if $Fr = \infty$ or $Fr = \epsilon^{-3}F$ where $F = O(1)$, the last term of equation (58) is zero and one solution of this equation is $q = 0$, i.e., $h_0 = C_2$, and, therefore, $B = \frac{1}{C_2}$, where C_2 is a constant which may be set to one without loss of generality. This is not surprising since $Fr = \infty$ and $Fr = \epsilon^{-3}F$ where $F = O(1)$ correspond to zero- and micro-gravity conditions, respectively. The linear stability of the steady state solution $h_0 = B = 1$ for $Fr = \infty$ is analysed in the next section.

Linear temporal stability for $Fr = \infty$

For $Fr = \infty$ or $Fr = \epsilon^{-3}F$ where $F = O(1)$, the stability of the steady state solution $h_0 = B = 1$ may be analysed by substituting

$$h_0 = 1 + H(x,t), \qquad B = 1 + b(x,t), \tag{59}$$

where $|H| \ll 1$ and $|b| \ll 1$, into equations (44) and (46) and neglecting the non-linear terms in the resulting equation. This yields the following system of linear, partial differential equations

$$\frac{\partial H}{\partial t} + \frac{\partial H}{\partial x} + \frac{\partial b}{\partial x} = 0, \tag{60}$$

$$R\left(\frac{\partial b}{\partial t} + \frac{\partial b}{\partial x}\right) = 4\frac{\partial^2 b}{\partial x^2} + \frac{1}{C}\frac{\partial^3 H}{\partial x^3} + 3A\frac{\partial H}{\partial x}. \tag{61}$$

Substitution of

$$H = \alpha e^{i(\omega t + kx)}, \qquad b = \beta e^{i(\omega t + kx)}, \tag{62}$$

where α and β are complex constants, $i^2 = -1$, k is the real wave number, and ω is the angular frequency, into equations (60) and (61) results in a system of homogeneous, linear algebraic equations for α and β which has a non-trivial solution if its determinant is identically equal to zero. This condition implies that

$$\omega = -k + \frac{2k^2}{R}\left(i \pm \left(\frac{R}{4C} - 1 - \frac{3AR}{4k^2}\right)^{\frac{1}{2}}\right), \tag{63}$$

which indicates that equations (60) and (61) are dispersive.

Small wavenumber asymptotics. If the wavenumber is small, i.e. $k << 1$, the wavelength is large, and equation (63) may be written asymptotically as

$$\omega = -k + \frac{2ik^2}{R} \pm ik\left(\frac{3A}{R}\right)^{\frac{1}{2}}\left(1 - \frac{R-4C}{6ARC}k^2 + O(k^4)\right), \tag{64}$$

which indicates that long waves are unstable on account of the ± sign if $A \neq 0$. If $A = 0$, long waves are stable.

Large wavenumber asymptotics. If the wavenumber is large, i.e. $k >> 1$, the wavelength is short, and equation (63) may be written asymptotically as

$$\omega = -k + \frac{2k^2}{R}\left(i \pm \left(\frac{R}{4C} - 1\right)^{\frac{1}{2}} + O(\frac{1}{k^2})\right), \tag{65}$$

provided that $R \neq 4C$.

Equation (65) indicates that short waves are stable provided that $R \neq 4C$. If $R = 4C$, waves with wavenumbers $k < \left(\frac{3AR}{4}\right)^{\frac{1}{2}}$ are unstable. If $A = 0$, short waves are stable.

Critical wavenumbers correspond to $\omega_I = 0$ where ω_I denotes the imaginary part of ω. Note that $\omega_I > 0$ implies stability, and that criticality corresponds to temporal oscillations according to equation (62). The radicand in equation (63) is negative for $k < \left(\frac{3ARC}{R-4C}\right)^{\frac{1}{2}}$ if $R \neq 4C$, which implies that, since k is a real number, R must be greater than $4C$. Therefore, if $R < 4C$, the planar liquid sheet is linearly unstable, whereas, if $R > 4C$, the critical wavenumber corresponds to $k_c = (3AC)^{\frac{1}{2}}$. If $R = 4C$, the critical wavenumber is $k_c = \left(\frac{3AR}{4}\right)^{\frac{1}{2}}$ and waves with $k < k_c$ are linearly unstable. If $A = 0$, all the waves are stable, while, if C = ∞, there is linear instability.

The temporal, linear stability analysis performed in this section clearly indicates that the London-van der Waals body forces may cause the rupture of planar liquid sheets. The stability analysis presented here may not be used to determine the film rupture because of its linearity. An accurate analysis of the rupture requires the use of non-linear methods and numerical techniques for the solution of equations (44) and (46) subject to appropriate initial and boundary conditions.

Presentation of results

Some sample results corresponding to steady, plane stagnation flows and film casting processes are presented when the London-van der Waals forces are of great importance and $C = \infty$. These results are to be compared with those of reference[3] where attractive body forces were not considered, and different flow approximations were analysed.

Steady, plane stagnation flows

For steady, plane stagnation flows, the boundary conditions at the nozzle exit and at the solid wall, i.e. at the downstream boundary, are

$$u_0(0) = h_0(0) = 1, \qquad u_0(1) = 0, \qquad h_0(1) = \infty. \tag{66}$$

Figure 1 shows the leading-order thickness and axial velocity component of the planar liquid sheet obtained from the numerical solution of equation (57) for $R = 1$ and different values of R/F and A. This equation was discretized by means of a conservative, second-order accurate, iterative method with $h_0(1) = 10^{39}$ until

$$\sum_{1}^{NI} \left(\left(u_i^{k+1} \right)^2 - \left(u_i^k \right)^2 \right) \leq tol, \tag{67}$$

where $tol = 10^{-12}$, k denotes the k-th iteration and NI is the number of grid points. In the calculations presented here, NI was varied until grid-independent results were obtained. In most of the calculations presented here, $NI = 1{,}000$ unless stated otherwise.

Since the leading-order thickness increases rapidly to ∞ at the downstream boundary, only a small fraction of the $h_0(x)$ curve is illustrated in Figure 1.

Figure 1 (top) shows that the leading-order thickness and axial velocity component of the planar liquid sheet are monotonically increasing and decreasing, respectively, functions of the axial co-ordinate for $R/F = 1$, and that the deceleration of the sheet decreases as the Hamaker constant is increased. Figure 1 (top) also shows very few differences between the curves corresponding to $A = 1$ and $A = 0.1$.

Similar trends to those illustrated in Figure 1 (top) have also been observed for $R/F = 0.01$, although for Reynolds-to-Froude number ratios less than one, the deceleration of the planar liquid sheet is larger and the effect of the Hamaker constant is less pronounced than those illustrated in Figure 1 (top), as shown in the middle graphs of Figure 1 which correspond to $R/F = 0.01$.

For Reynolds-to-Froude number ratios greater than one, neither the thickness nor the axial velocity component of the planar liquid sheet are monotonic functions of the axial co-ordinate as shown in Figure 1 (bottom). This figure indicates that, first, there is a contraction of the planar liquid sheet, followed by thickening. This figure also shows that the difference between the results corresponding to $A = 1$ and $A = 0.1$ are smaller than those between $A = 1$ and $A = 10$. In particular, a Hamaker constant greater than one results in a thickening of the planar liquid sheet closer to the downstream boundary than Hamaker's constants less than or equal to one. It must be noted that the London-van der Waals forces are inversely proportional to the third power of the leading-order thickness; therefore, these forces are most effective when the planar liquid sheet's thickness is smallest. As the sheet approaches the downstream boundary, its thickness increases and the effects of the London-van der Waals forces decrease as shown in the graph of the axial velocity component in Figure 1 (bottom).

Figure 2 shows the effects of the Reynolds number and Reynolds-to-Froude number ratio on the leading-order thickness and axial velocity component for $A = 1$ and different approximations to plane stagnation flows. These effects were determined with the full equation (57) and and $R = 1$, equation (57) with $R = 0$

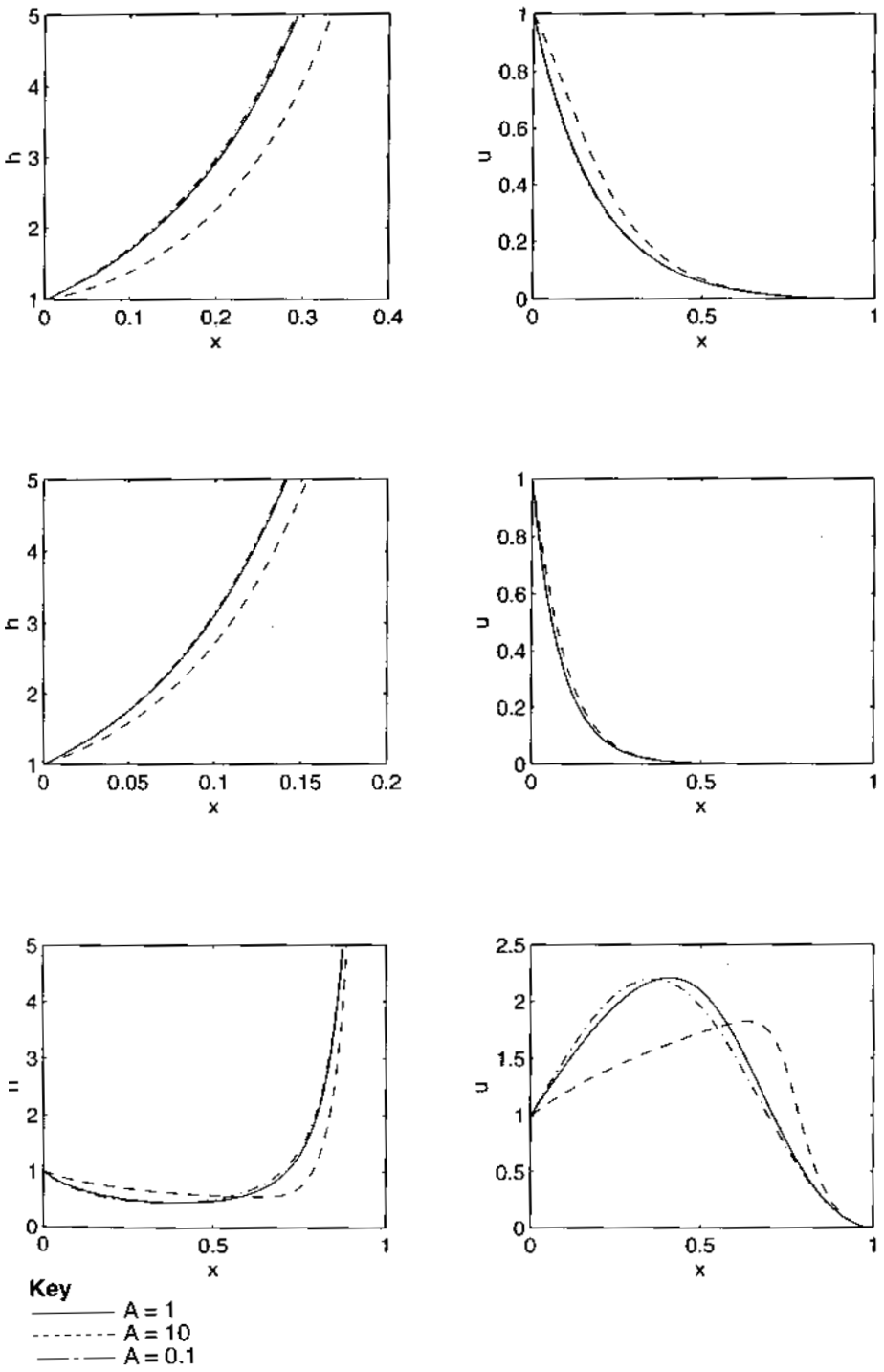

Figure 1.
Leading-order thickness (left) and axial velocity component (right) for plane stagnation flows. (Equation (57) with $C = 0$ and $R = 1$; top row: $R/F = 1$; middle row: $R/F = 0.01$; bottom row: $R/F = 100$.)

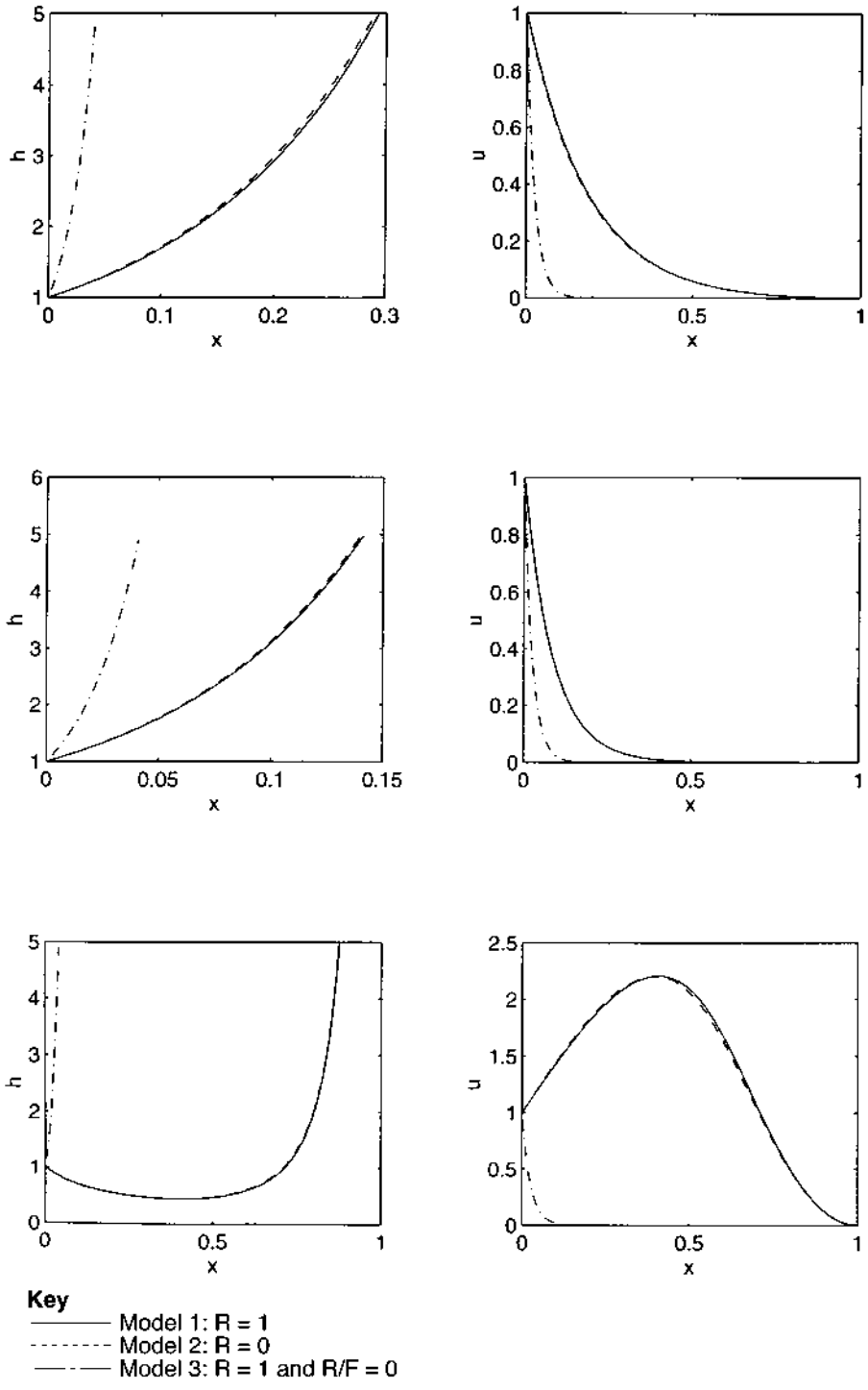

Figure 2. Leading-order thickness (left) and axial velocity component (right) for plane stagnation flows. (Equation (57) with $C = 0$ and $A = 1$; top row: $R/F = 1$ for models 1 and 2; middle row: $R/F = 0.01$ for models 1 and 2; bottom row: $R/F = 100$ for models 1 and 2.)

and finite values of R/F, and equation (57) with $R = 1$ and $R/F = 0$ which are here referred to as models 1, 2 and 3, respectively.

Figure 2 indicates that the differences between the results corresponding to models 1 and 2 are very small. This figure also shows that the thickening of the planar liquid sheet increases as the Froude number is decreased; this is a consequence of the gravitational pull as shown in the top and middle graphs of Figure 2 which indicate that the thickening of the planar liquid sheet increases and occurs further downstream as R/F is decreased. Figure 2 (bottom) shows a non-monotonic behaviour for models 1 and 2 and a monotonic one for model 3. The latter is a consequence of the fact that $R/F = 0$ in model 3. Note that, in Figure 2 (bottom), the sheet first contracts and then thickens for models 1 and 2, whereas it continually thickens for model 3.

Similar trends to those shown in Figure 2 have also been observed for $A = 10$ and 0.01, although the axial velocity component decelerates at a slower rate and the differences between models 1 and 2 increase as A is increased.

Steady film casting processes

Although film casting processes of very thin planar liquid sheets may be nearly impossible to carry out experimentally, the results presented in this section illustrate the effects of the downstream boundary conditions on the numerical solution of equation (57). This equation was solved by using the same boundary conditions at $x = 0$ as those of equation (64), the same numerical technique as that of the previous section, and different take-up or downstream boundary conditions.

Figure 3 correspond to model 1, $R = 1$, three different values of R/F, and two different take-up velocities. This figure shows that a boundary layer forms at the downstream boundary, and the thickness of this layer decreases as A is increased. In order to resolve this boundary layer accurately, 10,000 grid points were used in the numerical calculations. Similar trends to those shown in the plots of the first and second rows of Figure 3 have also been observed for $R/F \leq 0.01$; in fact, the differences between the results corresponding to the first and second rows of Figure 1 are not visible for the scale used in both figures.

The graphs in the third row of Figure 3 correspond to $R/F = 100$ and exhibit different trends to those of the first two rows. The latter show downward concavity in the leading order thickness for $A = 1$ and 10, and upward concavity for $A = 0.01$. By way of contrast, the curves presented in the third row of Figure 3 for $A = 1$ and 10 exhibit an inflection point in the leading-order thickness, and this point owes its presence to the large gravitational pull associated with small Froude numbers.

Similar trends to those shown in the first three rows of Figure 3 have also been observed for $u_0(1) \geq 100$, except that the thickness of the boundary layer at the downstream boundary decreases as $u_0(1)$ is increased as shown in the fourth row of Figure 3.

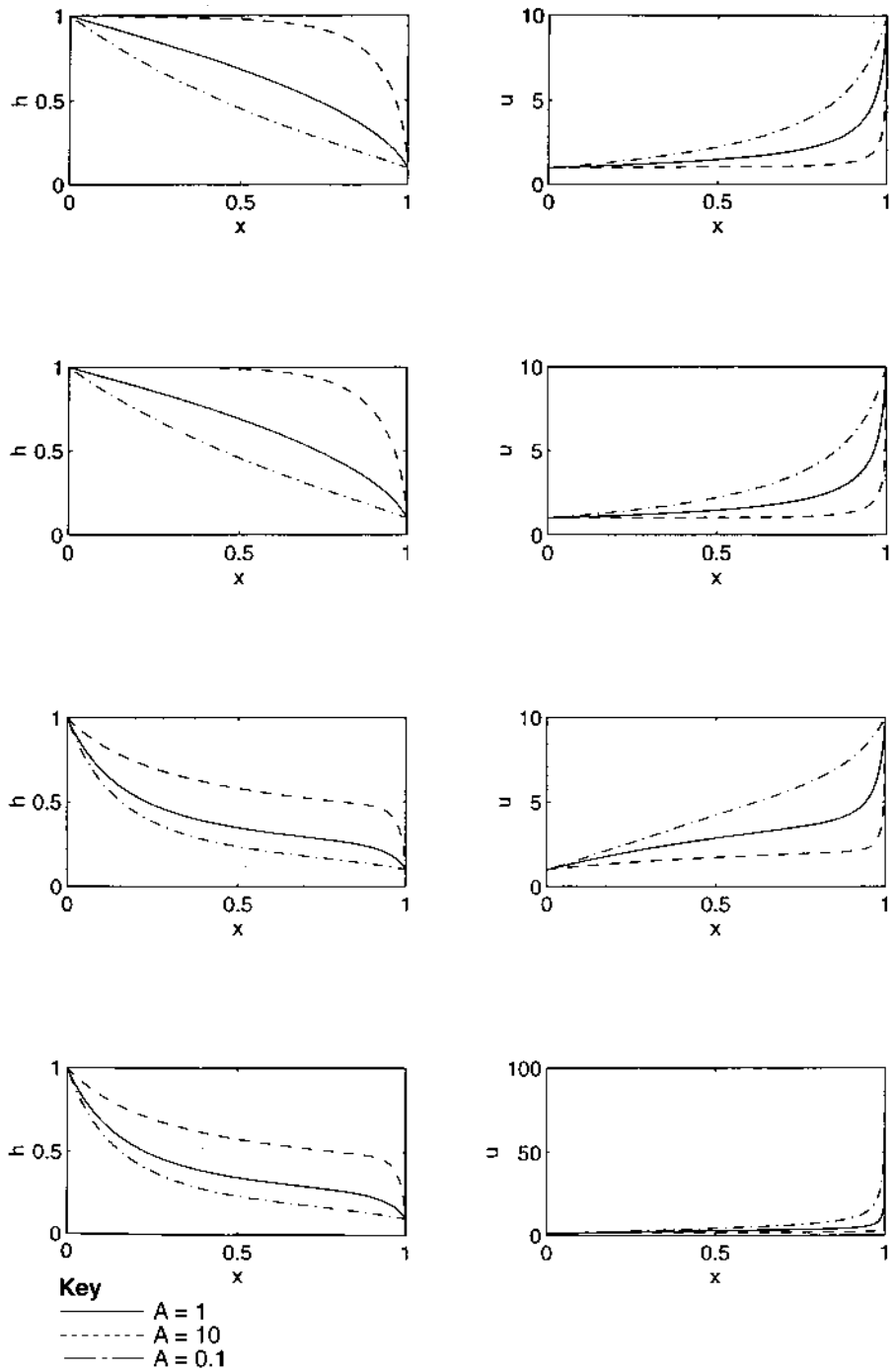

Figure 3. Leading-order thickness (left) and axial velocity component (right) for film casting processes. (Equation (57) with C = 0 and R = 1; first row from top: R/F = 1 and $u_0(1)$ = 10; second row from top: R/F = 0.01 and $u_0(1)$ = 10; third row from top: R/F = 100 and $u_0(1)$ = 10; fourth row from top: R/F = 100 and $u_0(1)$ = 100.)

Figure 4 illustrates the leading-order thickness and axial velocity component of the planar liquid sheet for the three models described in the previous section. This figure shows very small differences between the three models for $u_0(1) = 10$ and different values of A, and illustrates that model 3 predicts a slightly lower axial velocity component than models 1 and 2 due to the zero gravitational pull in that model, indicating that, for a take-up speed equal to ten, the effects of the gravitational pull are very small. The differences between the predictions of the three models increase as A is increased as indicated in the results presented in the third row of Figure 4. Similar trends to those shown in Figure 4 have also been observed for $u_0(1) = 100$.

Similar trends to those presented in Figure 4 have been noted for $R/F = 0.01$ as illustrated in Figure 5 which indicates that the differences between the models 1 and 3 are negligible for small Reynolds-to-Froude number ratios. This is again due to the fact that gravitational effects are almost negligible for the Froude numbers considered in Figure 5. However, as the magnitude of the Reynolds-to-Froude number ratio is increased, substantial differences between the three models considered in this paper can be noted as illustrated in Figure 6. For example, the first and second rows of this figure show that model 3 predicts a much slower axial velocity component than models 1 and 2. This is not at all surprising, for model 3 neglects the gravitational pull. Furthermore, both the leading-order thickness and axial velocity component predicted by models 1 and 2 exhibit inflection points, whereas the concavity of the predictions of model 3 is of the same sign. In addition, the thickness of the boundary layer predicted by model 3 is smaller than those predicted by models 1 and 2.

Conclusions

Asymptotic methods have been used to derive the long-wave equations governing the fluid dynamics of thin, free-falling, planar liquid sheets subject to London-van der Waals forces at low Reynolds numbers. It has been shown that, in order to include the effects of gravity, surface tension, viscosity and London-van der Waals body forces, the Reynolds and capillary numbers and Hamaker's constant must be small, whereas the Froude number must be large. It has also been shown that the dynamics of thin, free-falling, planar sheets are governed by two, non-linearly coupled, partial differential equations for the leading order film thickness and axial velocity component, in contrast with films on solid substrates whose dynamics is governed by only one partial differential equation for the film thickness.

Analytical solutions of the steady equations have been found for small surface tension and zero Reynolds number or large Froude numbers. A linear, temporal stability analysis of the leading order equations governing the dynamics of thin, planar sheets indicates that these sheets are unstable for certain wavenumbers. Since the analysis presented in the paper used symmetry conditions at the sheet centreline, it may be used to study the symmetric or varicose rupture of planar sheets.

Numerical studies of planar liquid sheets at low Reynolds numbers with no surface tension indicate that, for plane stagnation flows, the deceleration of the

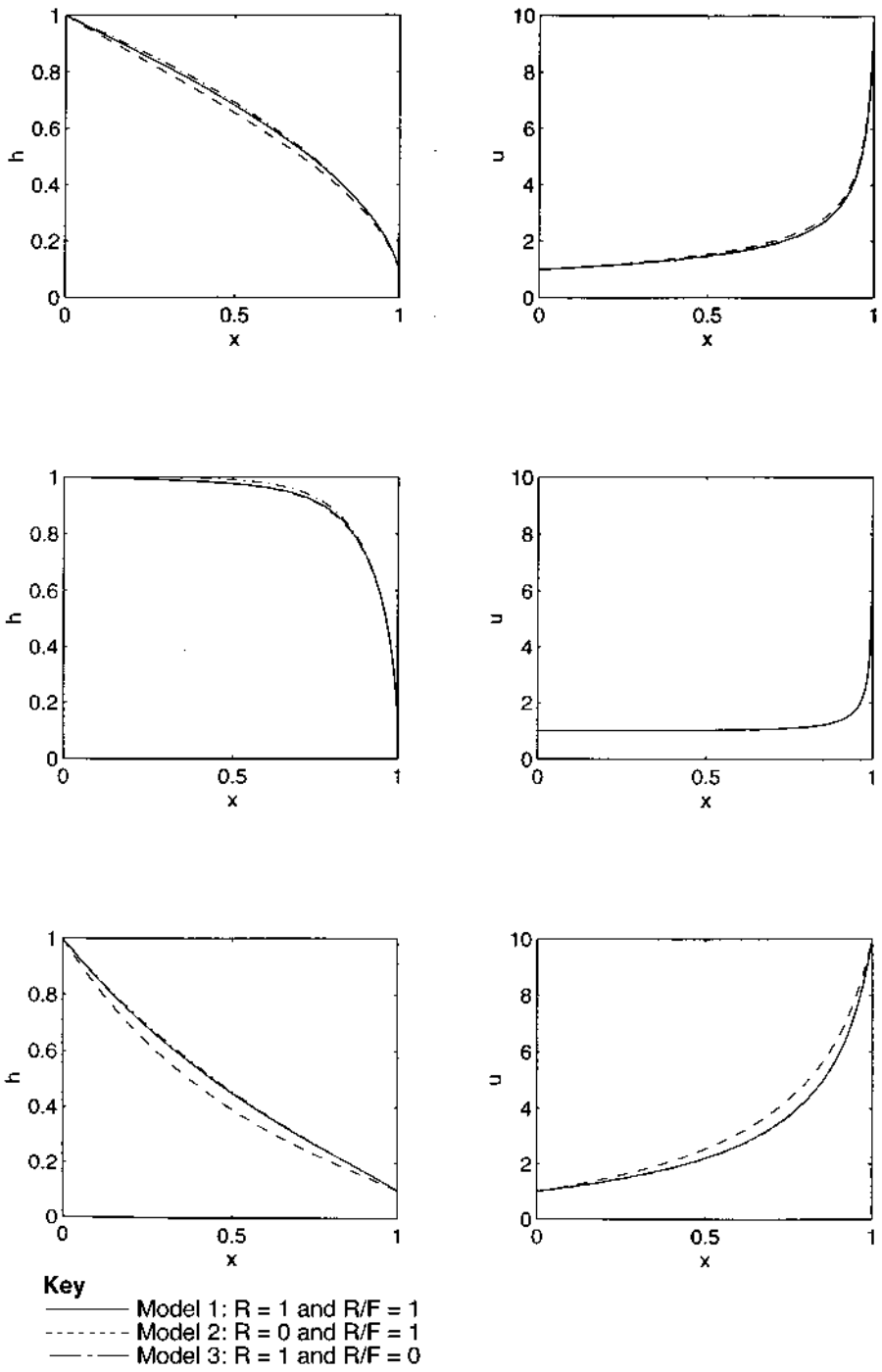

Figure 4. Leading-order thickness (left) and axial velocity component (right) for film casting processes. (Equation (57) with C = 0; top row: A =1; middle row: A = 10; bottom row: A = 0.1.)

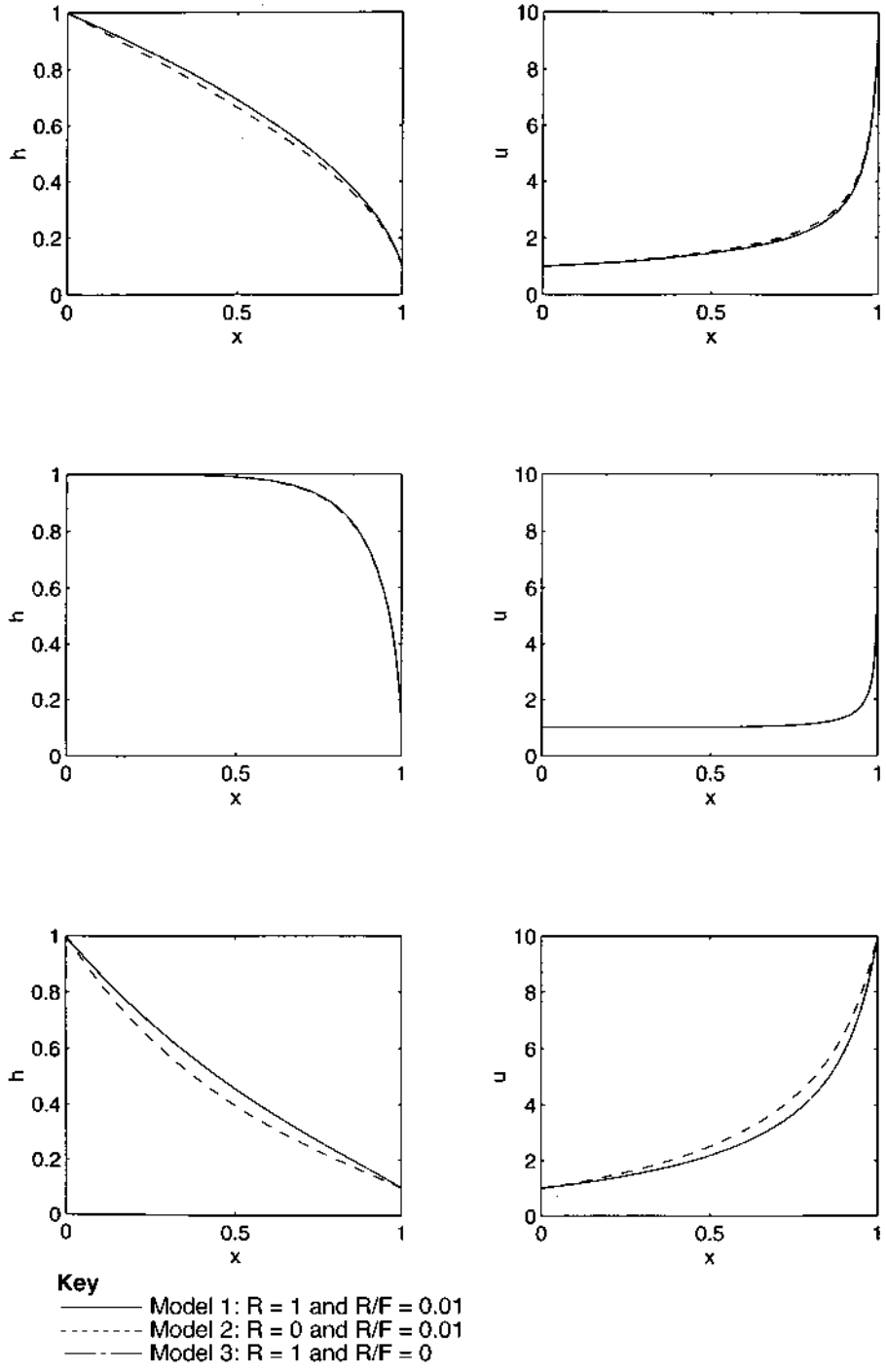

Figure 5.
Leading-order thickness (left) and axial velocity component (right) for film casting processes. (Equation (57) with C = 0; top row: A = 1; middle tow: A = 10; bottom row: A = 0.1.)

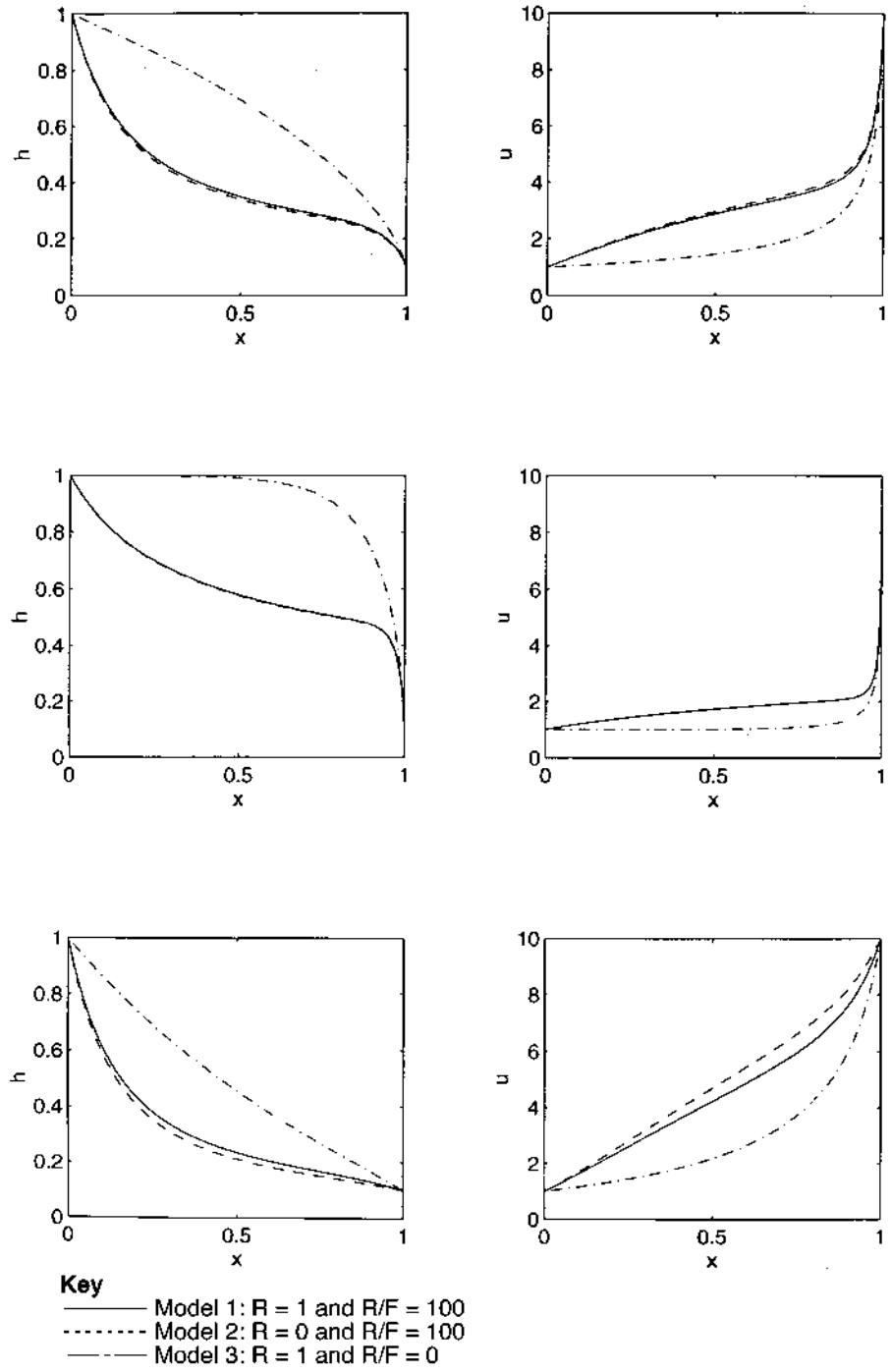

Figure 6. Leading-order thickness (left) and axial velocity component (right) for film casting processes. (Equation (57) with C = 0; top row: A = 1; middle row: A = 10; bottom row: A = 0.1.)

sheet as it approaches the solid wall decreases as the London-van der Waals forces are increased. This is a consequence of the fact that these forces are inversely proportional to the third power of the sheet's thickness. Furthermore, the effects of these body forces decrease as the Froude number is increased. For Reynolds-to-Froude numbers greater than one, it has been observed that the thickening of the sheet as it approaches the solid boundary increases as the Hamaker constant is increased.

Numerical experiments of film casting processes have also been performed in order to assess the effects of the attractive London-van der Waals forces and boundary conditions on the fluid dynamics of planar liquid sheets. These experiments indicate that, for high take-up speeds, a, boundary layer is formed at the downstream boundary, and the thickness of this layer decreases as the London-van der Waals forces are increased. For Reynolds-to-Froude numbers larger than one, it has been observed that both the leading-order thickness and axial velocity component are very sensitive to the value of the Hamaker constant. For Hamaker's constants less than one, the concavity of the leading-order thickness is of the same sign and, at most, exhibits an inflection point near to the downstream boundary. However, for Hamaker's constants equal to or larger than one, the leading-order thickness shows an inflection point near to the mid-point between the upstream and downstream boundaries.

Numerical experiments have also been performed with three different flow approximations which account for or neglect inertia and/or the gravitational pull. The results of these experiments indicate that these approximations produce very similar results for Reynolds-to-Froude number ratios equal to or less than one.

Acknowledgements

The research reported in this paper was supported by Project PB94-1494 from the DGICYT of Spain.

References

1. Ruschak, K.J., "Coating flows", *Annual Review of Fluid Mechanics*, Vol. 17, 1985, pp. 65-89.
2. Brown, D.R., "A study of the behaviour of a thin sheet of moving liquid", *Journal of Fluid Mechanics*, Vol. 10, 1961, pp. 297-305.
3. Ramos, J.I., "Planar liquid sheets at low Reynolds numbers", *International Journal for Numerical Methods in Fluids*, in press, 1995.
4. Israelchvili, J., *Intermolecular and Surface Forces*, 2nd ed., Academic Press, New York, NY, 1992.
5. Derjaguin, B.V., Churaev, N.V. and Muller, V.M., *Surface Forces,* Consultants Bureau, New York, NY, 1987.
6. Davis, S., "Rupture of thin films", in Meyer, R.E. (Ed.), *Waves on Fluid Interfaces*, Academic Press, New York, NY, 1983, pp. 291-302.
7. Slattery, J.C., *Interfacial Transport Phenomena*, Springer-Verlag, New York, NY, 1990.
8. Erneux, T. and Davis, S.H., "Nonlinear rupture of free films", *Physics of Fluids A: Fluid Dynamics*, Vol. 5, 1993, pp. 1,117-22.
9. Prudnikov, A.A., Brychkov, Y.A. and Marichev, O.I., *Integrals and Series, Volume 1: Elementary Functions,* Gordon and Breach, New York, NY, 1986.